Thermal and magnetic properties and density of state of in 3D SnTe (001) surface state under combined exchange and strain effects

Khaled Abdulhaq, Mohammad K. Elsaid, Diana Dahliah

Physics department, An-Najah National University, Nablus, Palestine

Corresponding author: Mohammad K. Elsaid, mkelsaid@najah.edu; Diana Dahliah, diana.dahliah@najah.edu

ABSTRACT This paper presents a comprehensive investigation of the essential properties of topological insulator materials like electronic, thermal, and magnetic quantities. We considered crystalline topological insulators tin telluride (SnTe), deposited on a magnetic substrate material. The anisotropic mass Hamiltonian is considered to obtain eigenenergy spectra expression in the presence of exchange proximity and strain effects. We showed that the strain has an important effect in shifting the position of the valley or Dirac points in the reciprocal space; an important result that leads to significant role in using the topological material as an electronic component in the new hot research area called valley electronics. We displayed the dependences of the computed density of states, heat capacity, and the magnetic susceptibility of the crystalline topological material, SnTe, on the Hamiltonian physical parameters.

KEYWORDS topology, SnTe, thermal properties, magnetic properties

FOR CITATION Abdulhaq K., Elsaid M.K., Dahliah D. Thermal and magnetic properties and density of state of in 3D SnTe (001) surface state under combined exchange and strain effects. *Nanosystems: Phys. Chem. Math.*, 2025, **16** (2), 199–208.

1. Introduction

Many aspects of condensed matter physics are related to classifying phases of matter [1, 2]. Over the past decades, the study of the quantum Hall effect has led to a different classification model, based on the notion of topological order. Recently, a new class of materials has been emerged which is called a topological insulator (TI) [3–5]. Topological insulators are electronic materials that have a bulk band gap like an ordinary insulator, but have protected conducting states on their edge or surface. Topological insulators come in various forms, including 2D topological insulators and 3D topological insulators, as well as topological superconductors, which have been investigated thoroughly qualitatively and quantitatively [6–8]. 3D topological insulators form a class of materials that exhibit interesting electronic properties, particularly in their surface states. These materials are insulators in the bulk, meaning that their interior does not conduct electricity. However, they have conductive surface states that are topologically protected [9]. The electronic properties of topological insulators are governed by their band structure, which is a representation of the allowed energy levels for electrons within the material. In a topological insulator, there is a band inversion between the valence and conduction bands, leading to the formation of surface states with a Dirac cone-like dispersion.

In topological crystalline insulators, the internal topology of the material preserving surface states are mirror symmetry, reflection symmetry, and rotational symmetry [10–13]. Additionally, there may be more than one symmetry types, some crystals have a group of symmetries depending on the crystal structure. It is important to note that these symmetries are dependent on the specific crystal lattice structure. In this paper, we are interested in SnTe crystal which is a topological crystalline insulator. The nontrivial topology in these crystals relies on the presence of reflection symmetry of the Rocksalt crystal structure with respect to the (110) mirror plane, and is mathematically characterized by an integer topological invariant the mirror Chern number [11]. Many researches were conducted to control the phase in Topological Crystalline Insulators TCIs via external factors such as temperature, symmetry breaking, strain, Rashba spin–orbit coupling, coupling to a ferromagnet, and charged impurities [10, 12, 14].

SnTe exhibits a naturally inverted band ordering, where the valence band originates from the cation Sn atoms, and the conduction band arises from Te atoms. This inversion, in contrast to a conventional ionic insulator, leads to the emergence of TCI phase in SnTe. SnTe is predicted to possess topological surface states on a set of crystal surfaces. Topological surface states on the (001) plane have been detected experimentally in angle-resolved photoemission spectroscopy (ARPES) investigations conducted on SnTe. Moreover, the spin texture observed in spin-resolved ARPES experiments offers a direct spectroscopic assessment of the mirror Chern number [11, 15].

On 2013, Yung Jui Wang, et al. conducted a first-principles calculations of the surface states in the CTI SnTe [5]. Timothy H. Hsieh et al. also showed that SnTe has metallic surface states with an even number of Dirac cones on high-symmetry crystal surfaces such as (001), (110) and (111) [10, 16].

By 2020, Researchers Pham, Binh, Viet, Dung, Hoi studied Rashba spin-orbit coupling (RSOC) effects on Dirac fermions in SnTe [17]. RSOC alters dispersion, group velocity and effective mass of the surface state electrons [17]. Hsieh et al. investigate the influence of breaking the mirror symmetry via external elastic strain or in-plane magnetic field [16]. On 2021, Ngo, Hieu, Lanh, Anh, and Hoi explored exchange field effects on the effective mass and the group velocity in SnTe/ferromagnet heterostructures [14].

SnTe has the potential, due to its unique electronics and thermoelectric properties, to make significant contributions to emerging technologies such as topological quantum computing and low power spintronics devices. Motivated by the noble material properties of SnTe, our aims to examine theoretically the properties of 3D CTI [18]. We will consider the Hamiltonian of surface state electrons under strain and exchange effects, and calculate energy levels via matrix diagonalization. The density of states will be computed using Green's functions. In addition, dynamic properties, group velocity and effective mass, will be investigated. The dynamic properties of the heterostructure of the topological SnTe/ferromagnetic device have not been thoroughly investigated theoretically for spintronic devices. In this paper, we explore these properties to assess the potential of SnTe.

The paper is organized as follows: In Section 2, we present theory. Section 3 shows results. Conclusion is presented in Section 4.

2. Theory and modeling

The surface states of the SnTe (001) TCI and related alloys around the x1 point can be described by the following effective Hamiltonian [8, 11, 18, 19]:

$$\widehat{H}_1(k) = v_1 k_x \sigma_y - v_2 k_y \sigma_x + n\tau_x + \delta\sigma_y\tau_y + M\sigma_z. \tag{1}$$

Here, the first two terms represent the Dirac model, resulting in energy linearly dependent on k, similar to photons. The third and fourth terms are to insure that the Hamiltonian of the (001) surface of SnTe must remain invariant under reflection along the x-axis, reflection along the y-axis, time-reversal symmetry. The last term signifies a mass term, arising from external factors like a ferromagnetic layer or an electric field. The values of the constants in this Hamiltoinan are as follows: the Fermi velocity along x-axis given by $\nu_1 = 1.3$ eV·Å and that along the y-axis equals to $\nu_2 = 2.4$ eV·Å. The two parameters $n = 0.07$ eV and $\delta = 0.026$ eV represent intervalley scattering at the lattice scale to reproduce the experimental observations [10, 18]. σ and τ are the Pauli matrices in spin and sublattice space.

The Hamiltonian in equation (1) can be diagonalized to find the energy levels:

$$E = \mu\sqrt{v_1^2 k_x^2 + v_2^2 k_y^2 + n^2 + \delta^2 + M^2 + 2v\sqrt{(n^2 + \delta^2)v_1^2 k_x^2 + n^2(v_2^2 k_y^2 + M^2)}}, \tag{2}$$

where $\mu = \pm 1$, $v = \mp 1$.

The strain in the 2D materials induces a pseudo-magnetic field, which can be represented in the Hamiltonian as a vector potential. This vector potential shifts the Dirac cones, allowing strain to control the position of the Dirac cones. Here, the same effect is seen, but due to the existence of multi-valley massless Dirac fermions at low energy, which appear as four Dirac points in the surface state (001). Each two of them have the same Hamiltonian because they are projected to the same surface momenta in the Brillouin zone. Therefore, two vector potentials should be included, and from the rotational symmetry between the Dirac points, knowing that the vector potentials are linearly proportional to strain field u_{ij}, then general formula of vector potentials [20, 21]:

$$\mathbf{A_1} = (\alpha_1 U_{xx} + \alpha_2 U_{yy}, \ \alpha_3 U_{xy}), \tag{3}$$

$$\mathbf{A_2} = (\alpha_3 U_{xy}, \ \alpha_1 U_{yy} + \alpha_2 U_{xx}). \tag{4}$$

Here α_1, α_2 and α_3 denote three independent constants. Knowing that the shear strain u_{xy} is very small with respect to U_{xx} and U_{yy}, U_{xy} can be ignored. The total vector potential can be written as:

$$\mathbf{A} = (\alpha_1 U_{xx} + \alpha_2 U_{yy}, \ \alpha_1 U_{yy} + \alpha_2 U_{xx}). \tag{5}$$

Then the shift in the momenta can be written as follows:

$$k_x \rightarrow k_x + \alpha_1 U_{xx} + \alpha_2 U_{yy}, \tag{6}$$

$$k_y \rightarrow k_y + \alpha_1 U_{yy} + \alpha_2 U_{xx}. \tag{7}$$

Under the influence of strain, the momentum will be shifted as expressed in Eqs. (6) and (7). Then, the energy dispersion relation of the SnTe (001) surface state under the influence of strain becomes:

$$E = \mu\sqrt{v_1^2(k_x + \alpha_1 U_{xx} + \alpha_2 U_{yy})^2 + v_2^2(k_y + \alpha_1 U_{yy} + \alpha_2 U_{xx})^2 + n^2 + \delta^2 + M^2 + 2vh(k)}, \tag{8}$$

where,

$$h(k) = \sqrt{(n^2 + \delta^2)\, v_1^2 \left(k_x + \alpha_1 U_{xx} + \alpha_2 U_{yy}\right)^2 + n^2 \left(v_2^2 \left(k_y + \alpha_1 U_{yy} + \alpha_2 U_{xx}\right)^2 + M^2\right)}. \tag{9}$$

The obtained energy in Eq. (8) will be used to calculate the band structure. Following this, the dynamic properties will be investigated, and the density of states using Green's functions will be computed. Thermal and magnetic properties will then be studied.

The partition function ($Z = \sum_n e^{-\beta E_n}$) is a fundamental and crucial quantity in statistical mechanics used to calculate thermal and magnetic properties.

The average energy is the average of all possible state at certain temperature which is defined as $\langle E \rangle = -\dfrac{\partial \ln(Z)}{\partial \beta}$. The average energy can be used to evaluate the magnetization, one of the most important magnetic properties, which indicates the response of the material's electrons' spin to an external magnetic field. It is defined as: $\langle \mathbf{M} \rangle = -\dfrac{\partial \langle E \rangle}{\partial B}$. Then, the magnetic susceptibility which classes the materials to diamagnetic ($\chi < 0$) and paramagnetic ($\chi > 0$), is defined as: $\chi = \dfrac{\partial \langle \mathbf{M} \rangle}{\partial B}$. It's also important to study the thermal properties to assess its thermal applications, such as whether the material acts as a thermal insulator or conductor, and whether it exhibits magnetocaloric properties. Magnetocaloric materials can be used for heating or cooling by applying a magnetic field.

Entropy is a measure of the disorder or randomness in a system, which can be used to check the magnetocaloric effect: $\langle S \rangle = \dfrac{\partial}{\partial T}\left(\dfrac{1}{\beta}\ln(Z)\right)$.

Dynamic properties such as group velocity $\mathbf{v_g} = \dfrac{1}{\hbar}\overrightarrow{\nabla_{\mathbf{k}}}E(k)$ and effective mass $m^* = \dfrac{\hbar^2}{\nabla_{\mathbf{k}}^2 E(k)}$ are essential properties for assessing the electronic applications of a material because the material's mobility depends on them.

Density of state which is the number of states per unit energy can give a lot of information about the band structure, Density of state mathematically is the delta function and it can be written in term of Green's function. Starting from the relationship between energy and wavefunction which is described by the Schrödinger equation $H\psi_n = E_n\psi_n$. The density of states can be expressed as the Dirac delta function of the energy: $D(E) = \sum_n \delta(E - E_n)$. The Green function is given by the following formula: $G = \dfrac{1}{E + i\varepsilon - H}$, where H is the Hamiltonian, E is the energy, and ε is very small real number.

Let us multiply the Green function by $|\psi_n\rangle$ from the right, and $\langle \psi_l |$ from the left and sum over all values of n and l. This results in:

$$\sum_{n,l}\langle \psi_l|\psi_n\rangle \frac{1}{E + i\varepsilon - E_n} = \sum_{n,l}\delta_{n,l}\frac{1}{E + i\varepsilon - E_n} = \sum_n \frac{1}{E + i\varepsilon - E_n}.$$

It is obvious that only the diagonal elements of the G matrix have non-zero values. To obtain the density of states from the Green function, let's take the imaginary part of the Green function, as follows:

$$\sum_n G_n = \sum_n \frac{1}{E - E_n + i\varepsilon}\frac{E - E_n - i\varepsilon}{E - E_n - i\varepsilon} = \sum_n \frac{E - E_n - i\varepsilon}{(E - E_n)^2 + \varepsilon^2}, \tag{10}$$

$$\sum_n \mathrm{Im}(G_n) = \sum_n -\frac{\varepsilon}{(E - E_n)^2 + \varepsilon^2}. \tag{11}$$

The Dirac delta function can be written in terms of the Lorentzian function, and the result is as follows:

$$DOS(E) = \sum_n \delta(E - E_n) = \lim_{\varepsilon \to 0} -\frac{1}{\pi}\sum_n \frac{\varepsilon}{(E - E_n)^2 + \varepsilon^2} = -\frac{1}{\pi}\lim_{\varepsilon \to 0}\sum_n \mathrm{Im}(G_n). \tag{12}$$

3. Results and discussions

In this section, we will study in detail the effects of strain on the main properties of the electrons. It is obvious from the strained Hamiltonian that the strain effect shifts the Dirac cone. Therefore, the strain effect can be utilized to control the properties of the SnTe (001) surface state.

In Fig. 1(a, and b), we used the strained dispersion relation to display the variation of the electron velocity as function of the strain. Fig. 1 represents the x-component of the group velocity of Dirac fermions at the Dirac point of momentum ($k_x = \sqrt{n^2 + \delta^2}/v_1$, $k_y = 0$), both in the first and second conduction states. In Fig. 1(a), the x-component of the group velocity is plotted as a function of U_{xx}. It is obvious that the x-component of group velocity changes with variations in U_{xx}. In the first conduction state, when U_{xx} is negative (tensile strain), the x-component of group velocity is negative and close to zero. However, with very small positive values of U_{xx} (compress strain), v_x remains negative and then it changes significantly and reach its minimum value as U_{xx} approaching $\sqrt{n^2 + \delta^2}/v_1$. Then, as U_{xx} increases v_x converges to small positive value which means that the electron wave is propagating along the positive x-direction. The observed behavior can be attributed to the role of strain as an effective vector potential within a specific range of applied strain or stress. In this regime, strain modifies the electronic band structure, leading to an increase in energy around the Dirac cone

as a function of momentum. Consequently, the group velocity, which is defined as the gradient of energy with respect to crystal momentum, aligns with the direction of the crystal momentum itself. This results in a conventional electron-like behavior, where charge carriers exhibit positive effective mass characteristics.
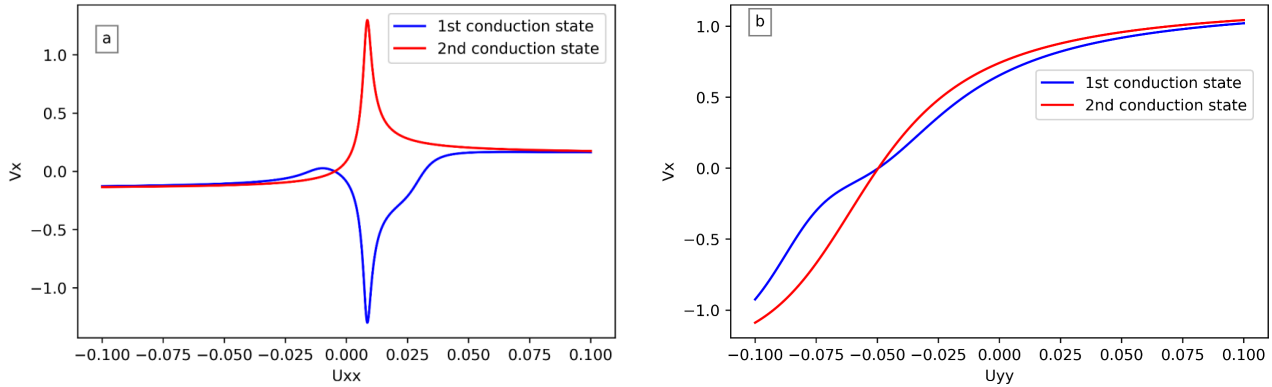

FIG. 1. x-component group velocity of Dirac fermions on SnTe (001) surface state with momentum $(\sqrt{n^2 + \delta^2}/v_1, \, 0)$ as a function of strain: (a) $U_{yy} = -0.04$; (b) $U_{xx} = 0.04$

However, if the applied strain or tensile deformation induces a shift in the Dirac point such that the crystal momentum is oriented opposite to the group velocity, the charge carriers within this regime will exhibit hole-like behavior. This phenomenon arises due to the band structure modification, where the energy-momentum dispersion relation is altered, effectively inverting the sign of the charge carrier velocity. In such cases, electrons in these regions behave similarly to holes, meaning they move as if they possess a positive charge within the material's electronic structure.

In the second conduction state when U_{xx} is negative/positive (tensile/compress strain), the x-component of group velocity converges to the same value as of the first conduction state. The only difference that around $U_{xx} = \sqrt{n^2+\delta^2}/v_1$. The group velocity changes drastically to reach its positive maximum.

Fig 1(b) represents the x-component of group velocity of Dirac fermions that have $(\sqrt{n^2 + \delta^2}/v_1, 0)$ momentum in the SnTe (001) surface state in the first and second conduction states as a function with U_{yy}, when U_{yy} is negative, both fermions in the first and second conduction states have a negative group velocity, and the value of the x-component of the group velocity of fermions in the first conduction state is greater than the x-component of the group velocity in the second conduction state. Near $U_{yy} = -0.05$ (i.e when $U_{yy} = -\sqrt{n^2+\delta^2}/v_1$) the group velocities in the first and second conduction states reach zero.

U_{yy} continues to increase, the x-component of the group velocity in both the first and second conduction states flips to positive values. At this critical value of U_{yy}, the wave propagation is switching from negative x-direction to positive one. Furthermore, the velocity becomes greater in the second conduction state. and as U_{yy} gets larger and larger the velocity in both bands converges to v_1.

Due to the importance of saddle points, the group velocity in the y-direction of the Dirac fermions at the saddle point is studied as a function of strain. Fig. 2 demonstrates the y-component of the group velocity as a function of strain tensor components. At the saddle points, there are no Dirac points in the y-direction, but the strain components affect the group velocity at the saddle point. If the strain is included as a vector potential, it shifts the Dirac points, affecting the entire band structure (breaking inversion symmetry). As a result, the energy, as a function of crystal momentum, changes. Within a certain range of strain, the energy increases as a function of crystal momentum, leading to a positive group velocity. Conversely, within another range of energy, the group velocity decreases as a function of crystal momentum, resulting in a negative group velocity. Notice, if $U_{yy} < -0.123$, the y-component of the group velocity of the Dirac fermions in both the first and second conduction states is negative (the energy decrease as a function of crystal momentum), and the fermions in the second conduction state have a greater group velocity. At $U_{yy} = 0.0123$, the group velocity of fermions in both states vanishes. If $U_{yy} > 0.0123$ the y-component of the group velocity of fermions in both states becomes positive (the energy increases as a function of crystal momentum).

Figure 2(b) represents the y-component of the group velocity of the Dirac fermions, at the saddle point in the first and second conduction states, as a function of U_{yy}. The y-component of the group velocity in both conduction states is positive, fermions in the second conduction state have greater y-component group velocity when $U_{yy} < -0.047$. For $-0.047 < U_{yy} < 0.029$, fermions in the first conduction state have a greater y-component group velocity, while for $U_{yy} > 0.029$, fermions in the second conduction state have a greater y-component group velocity

As has been mentioned earlier, the strain effect shifts the Dirac cone, which can be used to tune the properties of the surface state Dirac fermions in SnTe (001). One of the most important parameters for understanding the behavior of fermions is effective mass. Effective mass (which is the mass of electrons in the crystal) is the dynamical quantity which
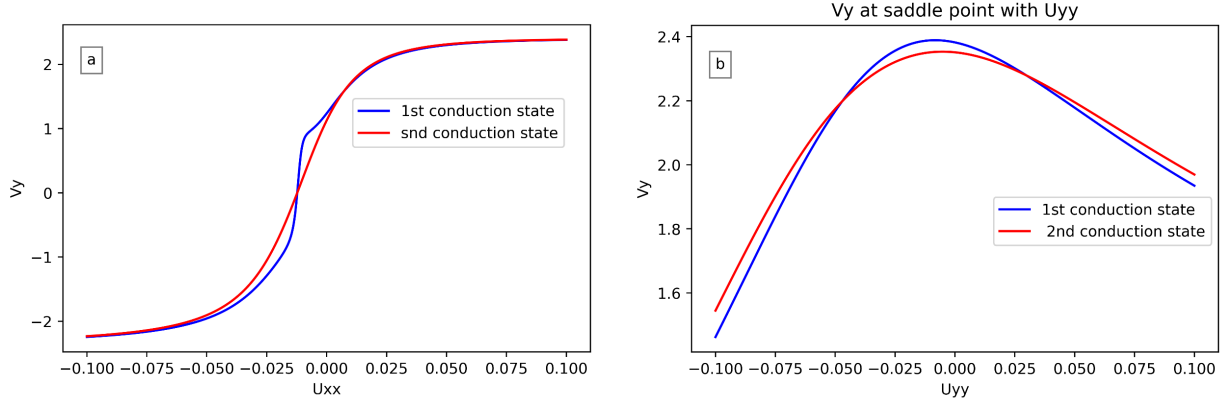
FIG. 2. y-component group velocity of Dirac fermions on SnTe (001) surface state that have $(0, \, n/v_2)$ momentum as a function of strain: (a) $U_{yy} = -0.04$; (b) $U_{xx} = 0.04$

is equal the reciprocal of the second derivative of the energy with respect to the crystal momentum. Fig. 3 represents the reciprocal of the effective mass in the x-direction for electrons in the conduction band as a function of strain tensor components at the Dirac point. The sign of the effective mass is determined by the curvature of the energy spectrum. In the first conduction state, the electrons are highly massive and behave like electrons due to the positive sign of the effective mass for $U_{xx} < -0.015$. However, when the energy is concave down the sign of the effective mass is negative as the first conduction band in Fig. 3(a), and the electrons behave like holes (they move in opposite direction to field lines in an electric field). In the range of $-0.015 < U_{xx} < 0.031$, the sign of the effective mass is negative, due to the downward concavity in the band curve in this region. So electrons behave like holes. Within this range of strain, the effective mass reaches two minimum values: one at $U_{xx} = 0.0063$ which is the absolute minimum and the other one at $U_{xx} = 0.011$. When $U_{xx} > 0.031$ the sign of the effective mass becomes positive again, and electrons behave like electrons, exhibiting high mass.
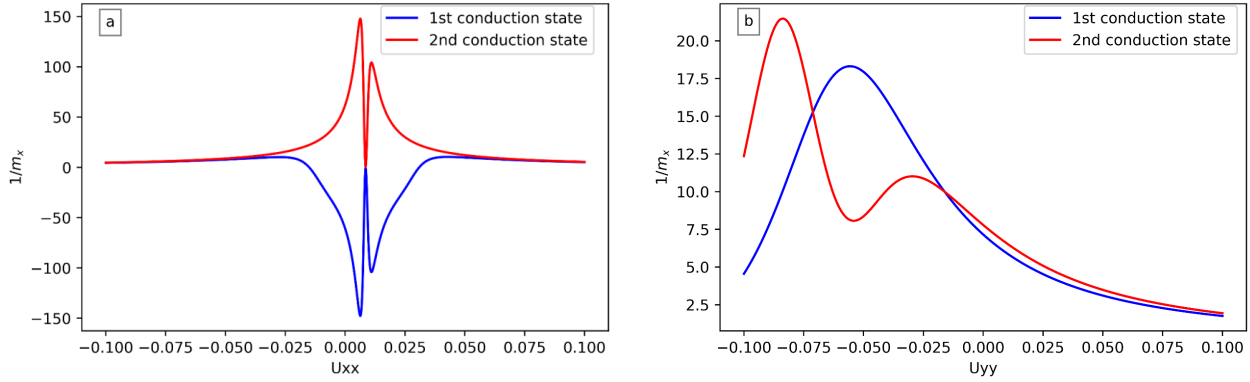

FIG. 3. Reciprocal effective mass in x-direction of the Dirac fermions on SnTe (001) surface state that have $(\dfrac{\sqrt{n^2 + \delta^2}}{v_1}, \, 0)$ momentum as a function of strain: (a) $U_{yy} = -0.04$, (b) $U_{xx} = 0.04$

In the second conduction state, the sign of the effective mass of Dirac fermions is positive for the strain range of $-0.1 < U_{xx} < 0.1$, indicating that electrons behave normally. However, in the range $U_{xx} < -0.015$ and $U_{xx} > 0.011$, the electrons exhibit high effective mass. The effective mass reaches its minimum values in the range of $-0.015 < U_{xx} < 0.011$ with one minimum at $U_{xx} = 0.0063$ which is the absolute minimum and the other one is at $U_{xx} = 0.011$.

Figure 3(b) represents the reciprocal effective mass in x-direction of Dirac fermions with $\sqrt{n^2 + \delta^2}/v_1$, 0) momentum as a function of U_{yy}, at $U_{xx} = 0.04$ in the first and second conduction states, in both states the sign of effective mass is positive so the electrons behave normally in these states.

When $U_{yy} < -0.56$, the effective mass in y-direction in the first conduction state decreases until it reaches its minimum value at $U_{yy} = -0.56$. when $U_{yy} > -0.56$ the effective mass increases.

In the second conduction state, the effective mass decreases when $U_{yy} < -0.084$, at this point the effective mass reaches an absolute minimum, for $-0.084 < U_{yy} < -0.054$, the effective mass increases. For $-0.054 < U_{yy} < -0.0295$,

the effective mass decreases again and reaches second minimum value at $U_{yy} = -0.0295$. When $U_{yy} > -0.0295$, the effective mass increases once more.

Figure 4(a and b) shows the effective mass in the y-direction at the saddle point as a function of the strain tensor components. The effective mass for both the first and second conduction states is positive, indicating that the energy states are concave up as a function of crystal momentum, and the electrons behave normally. In the first conduction state, the effective mass reaches an absolute minimum at $U_{xx} = -0.012$, and there is another minimum value of the effective mass at $U_{xx} = 0$. In the second conduction state, there is a minimum value at $U_{xx} = -0.011$. The effective mass can be negative only in the x-direction and for electrons in the first conduction state. This occurs because, in topological insulators, the first energy state bends only between the two Dirac points in the first conduction state.
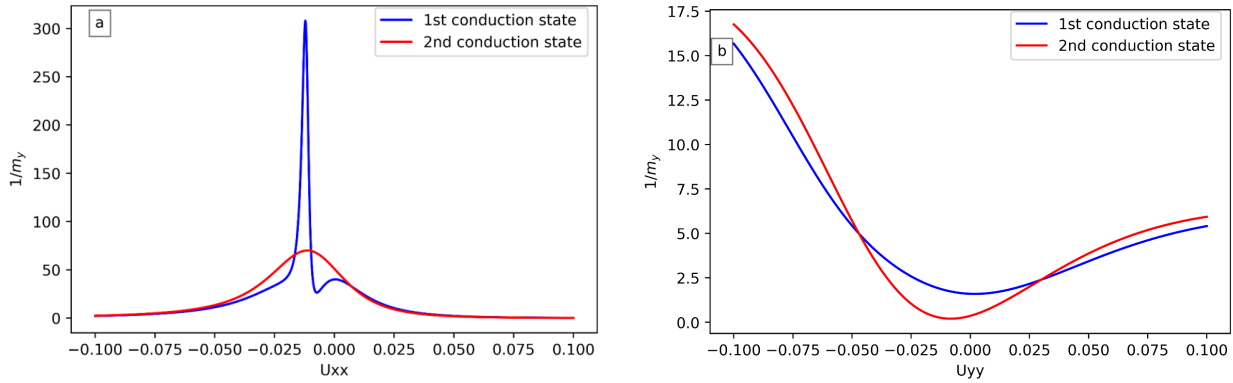

FIG. 4. Reciprocal effective mass in y-direction of the Dirac fermions on SnTe (001) surface state at the saddle point as a function of strain: (a) $U_{yy} = -0.04$; (b) $U_{xx} = 0.04$

Figure 4(b) represents the effective mass in y-direction as a function of U_{yy} at $U_{xx} = 0.04$, in both the first and second conduction states, the sign of the effective mass is positive, so the electrons behave like electrons.

In the first conduction state, the effective mass increases when $U_{yy} < 0.0019$, at $U_{yy} = 0.0019$ the effective mass reaches its maximum value. Then, when $U_{yy} > 0.0019$ the effective mass decreases.

In the second conduction state, the effective mass of Dirac fermions exhibits the same behavior, but it reaches its maximum value at $U_{yy} = -0.0083$. It's worth noting that the effective mass in the first conduction state is greater than that in the second conduction state when $-0.05 < U_{yy} < 0.028$, However, the effective mass in the second conduction state is greater when $U_{yy} < -0.05$ and $U_{yy} > 0.028$. In typical materials, the group velocity and the effective mass usually have the same sign. However, this can change in the presence of strong structural inversion asymmetry, which can arise due to spin-orbit interaction or strain, as in our case. By comparing our first four figures, we can identify regions where the signs of the effective mass and the group velocity differ.

4. Density of state of the Dirac fermions in 3D SnTe (001) surface state under combined exchange and strain effects

Density of state $D(E)$, which represents the number of states per unit energy, is a fundamental characteristics in solid state physics and condensed matter. It is used to study the electronic structure and the carrier concentration, which, in turn, determine the type of matter and its conductivity. Therefore, the density of state of the Dirac fermions in SnTe (001) surface state will be explored in this section.

Figure 5 displays the density of states $D(E)$ of the Dirac fermion surface states as a function of energy. Fig. 5(a) represents the pristine SnTe density of states, which is zero at zero energy and has a maximum value at $E = \pm\delta$, known as the Van Hove singularities. It is expected that the density of states has a maximum at $E = \pm\delta$ due to these being the energy values of the saddle points, and it has a local minimum at $E = \pm\sqrt{n^2 + \delta^2}$ located at $K = 0$.

Including the exchange effect ($M \neq 0$) which is a ferromagnetic substrate in our case, opens up an energy band gap E_g. Within this band gap, the density of states effectively approaches zero, as illustrated in Fig. 5(b). It's important to note that, as the exchange effect increases, the band gap widens, consequently expanding the energy range associated with zero density of states, the minimum point shift to the right. The density of state value at $E = \pm\delta$ increases when $-0.056 < M < 0.056$ and decreases when $M < -0.056$ and $M > 0.056$ as obvious in Fig. 6 which represent the density of state as a function of exchange effect when $E = \pm\delta$.

Figures 5(c and d) represents the density of states as a function of energy under the effect of x-direction uniaxial strain U_{xx} and y-direction uniaxial strain U_{yy}. The density of states at Van Hoove singularities decreases with strain, indicating a decrease in the concavity of the bands in the y-direction. The Dirac points along the x-direction remain when the strain is small, but as the strain becomes sufficiently strong, the Dirac points are destroyed and an energy gap opens in
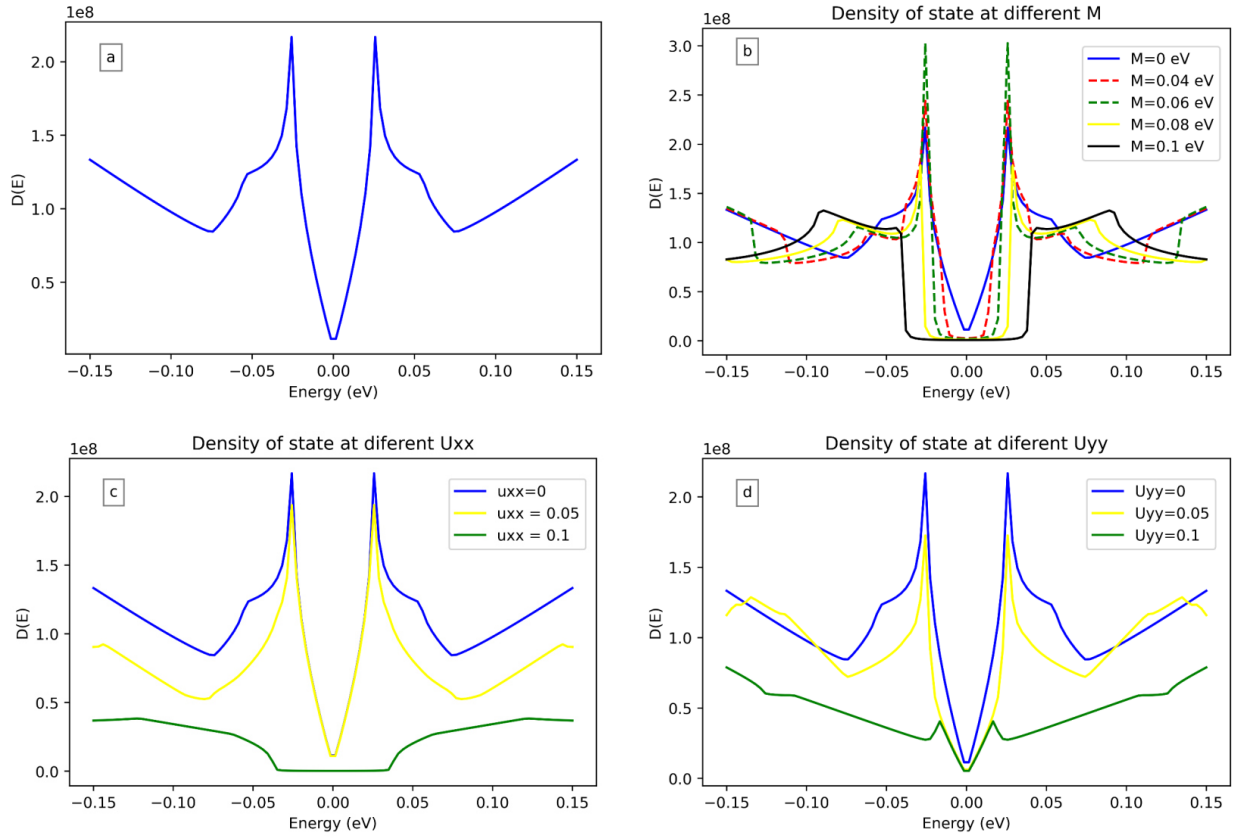
FIG. 5. Density of state of the Dirac fermions in SnTe (001) surface state as a function of energy: (a) Pristine SnTe; (b) at different values of M and zero strains; (c) at different values of uniaxial strain U_{xx}, $U_{yy} = 0$ and $M = 0$; (d) at different values of uniaxial strain U_{yy}, $U_{xx} = 0$ and $M = 0$
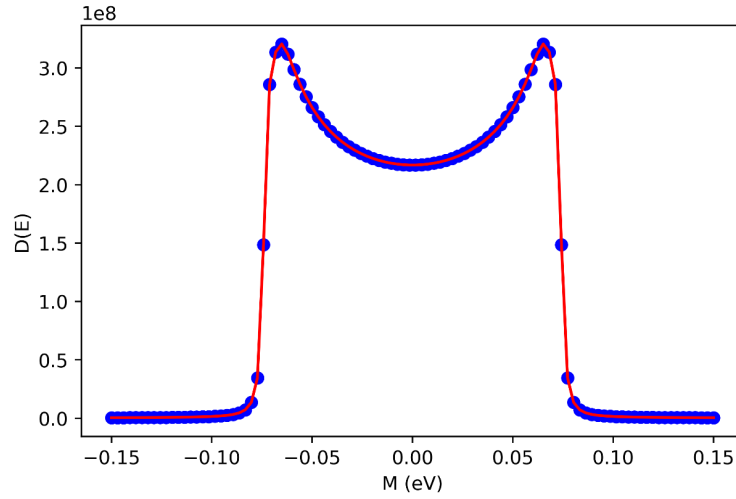

FIG. 6. Density of state of the Dirac fermions of SnTe (001) surface state as a function of exchange effect at $E = \pm\delta$

the x-direction. This effect becomes evident when $U_{xx} = 0.1$. Additionally, the minimum, located at $E = \pm\sqrt{n^2 + \delta^2}$ and $k = 0$, disappears when the strain becomes large enough.

5.   Thermal properties of Dirac fermions of SnTe (001) surface state

Due to the importance of the thermal properties in thermal applications such as heating or cooling and thermal insulation, in this section, thermal properties such as heat capacity and entropy of the SnTe (001) surface state will be discussed.

The heat capacity represents the first derivative of the average energy with respect to temperature. Fig. 7 shows the heat capacity as a function of temperature, with Fig. 7(a) showing the heat capacity at different values of the exchange effect. When $M = 0$, the Schottky anomaly point which corresponds to the peak in the heat capacity curve occurs at 451.52 K. When M changes to 0.02 and $M = 0.04$, the Schottky anomaly point shifts to the right; when $M = 0.06$ and $M = 0.08$, it shifts to the left. Interestingly, when $M = 0.1$, the Schottky anomaly point shifts to the right again, as evident in Table 1. The heat capacity decreases as M increases (for $M = 0.02, 0.04, 0.06,$ and 0.08). As the exchange effect increases, the heat capacity decreases. This occurs because the exchange effect opens an energy band gap, shifting the conduction states to higher energies. At low temperatures, the available thermal energy (given by K_BT) is small, making the higher-energy electronic states inaccessible.
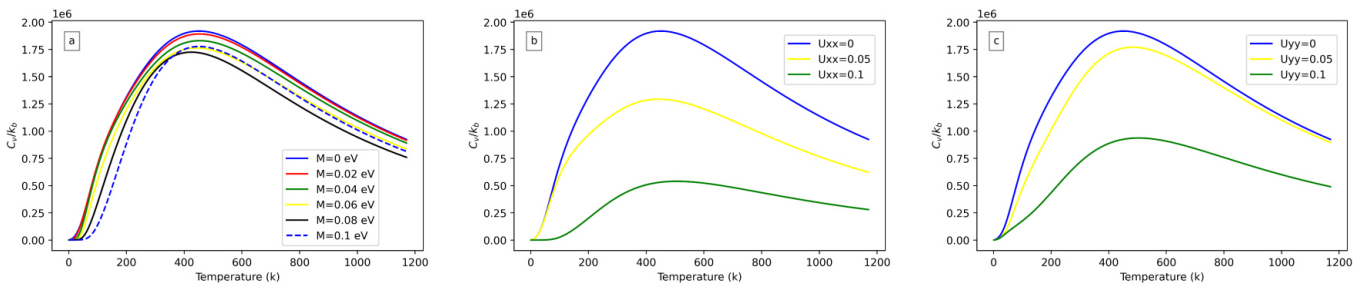

FIG. 7. Heat capacity of the Dirac fermions of SnTe(01) surface state as a function of temperature (a) at various values of exchange effect; (b) at different values of uniaxial strain in x-direction U_{xx}; (c) at different values of uniaxial strain in y-direction U_{yy}

TABLE 1. Temperature of the Schottky anomaly point at different values of the exchange effect (M)

M	0	0.02	0.04	0.06	0.08	0.1
Temperature (K)	451.51	452.69	453.86	442.15	424.6	451.51

Figure 7(b and c) represents the heat capacity of the Dirac fermions at different values of uniaxial strain in x-direction and in y-direction. It is found that in both cases the heat capacity decreases when increasing the strain and the Schottky anomaly point shifts as indicated in Tables 2 and 3. This occurs because the strain increasing shifts the Dirac points to higher values of crystal momentum, leading to a decrease in the density of states, as shown in Fig. 5(b and c). Since the heat capacity is proportional to $D(E)$, its value is reduced by decreasing of $D(E)$.

TABLE 2. Temperature of the Schottky anomaly point at different values of uniaxial x-direction strain (U_{xx})

U_{xx}	0	0.05	0.1
Temperature (K)	451.51	444.49	506.51

TABLE 3. Temperature of the Schottky anomaly point at different values of uniaxial y-direction strain (U_{yy})

U_{yy}	0	0.05	0.1
Temperature (K)	451.51	484.28	504.17

Entropy is an important quantity in thermodynamics, predicting the direction of spontaneous processes, such as heat transfer, chemical reactions, and phase changes. In statistical mechanics, it provides a bridge between the macroscopic

properties and microscopic configurations of a system, because it can be defined as the number of microscopic configurations consistent with a given macroscopic state of a system. Here the entropy of the Dirac fermions in SnTe (001) surface state will be studied.

Figure 8 represents the entropy as a function of temperature at different values of the exchange effect (Fig. 8(a)) and uniaxial strain (Fig. 8(b,c)), all these effects have the same qualitative influence on the entropy of the system: they decrease the entropy of the Dirac fermions. This occurs due to a decrease in the disordering of the system. Note that the entropy decreases more significantly when the strain is applied in the x-direction as shown in Fig. 8(b), in contrast to the y-direction as in Fig. 8(c).
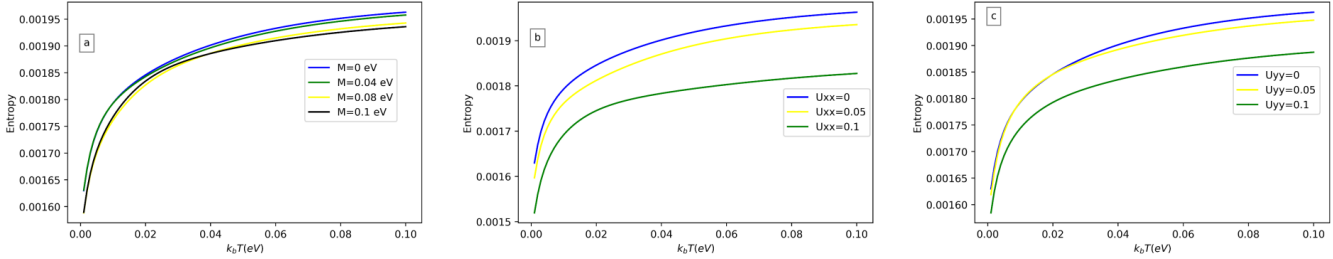

FIG. 8. Entropy of the Dirac fermions in SnTe (001) surface state as a function of temperature: (a) at different values of the exchange effect; (b) at different values of x-direction strain U_{xx}; (c) at different values of y-direction strain U_{yy}

6. Magnetic properties of the Dirac fermions of 3D SnTe (001) surface state

Magnetic properties such as magnetization M and magnetic susceptibility X are important in applications such as magnetic devices, sensors, detectors, and data storage. Magnetic susceptibility, which classifies materials into paramagnetic ($X > 0$) and diamagnetic ($X < 0$) categories, will be calculated.

Figure 9 represents the magnetic susceptibility as a function of temperature at different exchange effects and various uniaxial strain values. SnTe is a paramagnetic material since its magnetic susceptibility is greater than zero. However, the magnetic susceptibility decreases with increasing exchange effect or uniaxial strain, yet it remains greater than zero. Thus, SnTe remains paramagnetic under the influence of both the exchange effect and uniaxial strains. In Dirac materials, the magnetic susceptibility is zero because two conduction bands are identical. It means that there are no single electrons. However, in topological insulators, these identical states split into two spin-dependent states, leading to the presence of single electrons, which results in a magnetic susceptibility greater than zero. As the exchange effect or strain tensor components increase, the density of states decreases, reducing the number of single electrons and consequently decreasing the magnetic susceptibility.
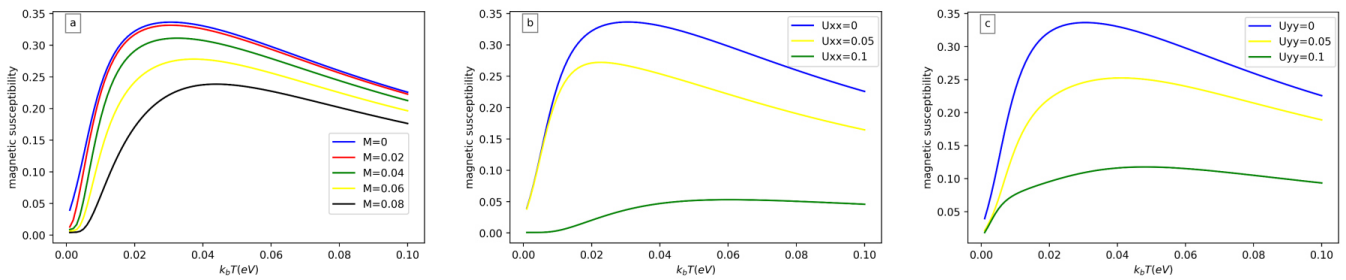

FIG. 9. Magnetic susceptibility of the Dirac fermions at SnTe (001) surface state as a function of temperature at (a) different value of exchange effect; (b) different values of uniaxial strain in x-direction U_{xx}; (c) different values of uniaxial strain in y-direction U_{yy}

7. Conclusion

This study has provided a comprehensive theoretical investigation into the electronic, thermal, and magnetic properties of topological insulators. By analyzing crystalline topological insulator SnTe, we have gained valuable insights into the behavior of these materials under different conditions. Our analysis revealed significant alterations in electronic properties due to the effects of exchange and strain. The examination of the group velocity, the effective mass, and the density of states provided a detailed understanding of its electronic structure. Furthermore, our investigation into thermal

and magnetic properties shed light on its potential applications in diverse fields, ranging from electronics to magnetism. It's obvious that the strain effect and the exchange effect can be used to control the properties of SnTe.

References

[1] Moore J.E. The birth of topological insulators. *Nature*, 2010, **464** (7286), P. 194–198.

[2] Qi, Xiao-Liang, Shou-Cheng Zhang. Topological insulators and superconductors. *Reviews of Modern Physics*, 2011, **83** (4), P. 1057–1110.

[3] Moore J. The next generation. *Nature Physics*, 2009, **5** (6), P. 378–380.

[4] Zhang, Haijun, et al. Topological insulators in Bi_2Se_3, Bi_2Te_3 and Sb_2Te_3 with a single Dirac cone on the surface. *Nature Physics*, 2009, **5** (6), P. 438–442.

[5] Hasan, Zahid M., Moore J.E. Three-dimensional topological insulators. *Annu. Rev. Condens. Matter Phys.*, 2011, **2** (1), P. 55–78.

[6] Batra, Navketan, Goutam Sheet. Physics with coffee and doughnuts: Understanding the physics behind topological insulators through Su-Schrieffer-Heeger model. *Resonance*, 2020, **25** (6), P. 765–786.

[7] Boothroyd A.T. Topological electronic bands in crystalline solids. *Contemporary Physics*, 2022, **63** (4), P. 305–327.

[8] Furchi, Marco, et al. Microcavity-integrated graphene photodetector. *Nano Letters*, 2012, **12** (6), P. 2773–2777.

[9] Ma, Eric Yue, et al. Unexpected edge conduction in mercury telluride quantum wells under broken time-reversal symmetry. *Nature Communications*, 2015, **6** (1), 7252.

[10] Xu, Su-Yang, et al. Observation of a topological crystalline insulator phase and topological phase transition in $Pb_{1-x}Sn_x$Te. *Nature Communications*, 2012, **3** (1), 1192.

[11] Tanaka Y., et al. Experimental realization of a topological crystalline insulator in SnTe. *Nature Physics*, 2012, **8** (11), P. 800–803.

[12] Dziawa P., et al. Topological crystalline insulator states in $Pb_{1-x}Sn_x$Se. *Nature Materials*, 2012, **11** (12), P. 1023–1027.

[13] Hsieh, Timothy H., et al. Topological crystalline insulators in the SnTe material class. *Nature Communications*, 2012, **3** (1), 982.

[14] Ngo B.V.Q., et al. Exchange field effects on the electronic properties of heterostructured ferromagnetic/topological crystalline insulator. *Physica E: Low-dimensional Systems and Nanostructures*, 2021, **126**, 114441.

[15] Liu, Junwei, Wenhui Duan, Liang Fu. Two types of surface states in topological crystalline insulators. *Physical Review B – Condensed Matter and Materials Physics*, 2013, **88** (24), 241303.

[16] Hsieh D., Xia Y., Wray L., Qian D., Pal A., Dil J. H., Osterwalder J., Meier F., Bihlmayer G., Hasan M.Z. Observation of unconventional quantum spin textures in topological insulators. *Science*, 2009, **323** (5916), P. 919–922.

[17] Pham, Khang D., et al. Controlling anisotropic surface group velocity and effective mass in topological crystalline insulator SnTe by Rashba effect. *Physica E: Low-dimensional Systems and Nanostructures*, 2020, **120**, 114118.

[18] Mitchell D.L., Wallis R.F. Theoretical energy-band parameters for the lead salts. *Physical Review*, 1966, **151** (2), 581.

[19] Ando, Yoichi, Liang Fu. Topological crystalline insulators and topological superconductors: From concepts to materials. *Annu. Rev. Condens. Matter Phys.*, 2015, **6** (1), P. 361–381.

[20] Tang, Evelyn, Liang Fu. Strain-induced partially flat band, helical snake states and interface superconductivity in topological crystalline insulators. *Nature Physics*, 2014, **10** (12), P. 964–969.

[21] Tien, Tong S., Pham TC Van, Le P.T.T. The strain and electric field modulation of magnetic properties in topological crystalline insulator thin films. *Chemical Physics Letters*, 2020, **751**, 137512.

Information about the authors:

Khaled Abdulhaq – Physics department, An-Najah National University, Nablus, Palestine; khaled.j.abdulhaq@gmail.com

Mohammad K. Elsaid – Physics department, An-Najah National University, Nablus, Palestine; ORCID 0000-0002-1392-3192; mkelsaid@najah.edu

Diana Dahliah – Physics department, An-Najah National University, Nablus, Palestine; ORCID 0000-0002-6919-3539; diana.dahliah@najah.edu

Conflict of interest: the authors declare no conflict of interest.